Article

Cell Reports

Apicobasal Polarity Controls Lymphocyte Adhesion to Hepatic Epithelial Cells

Graphical Abstract

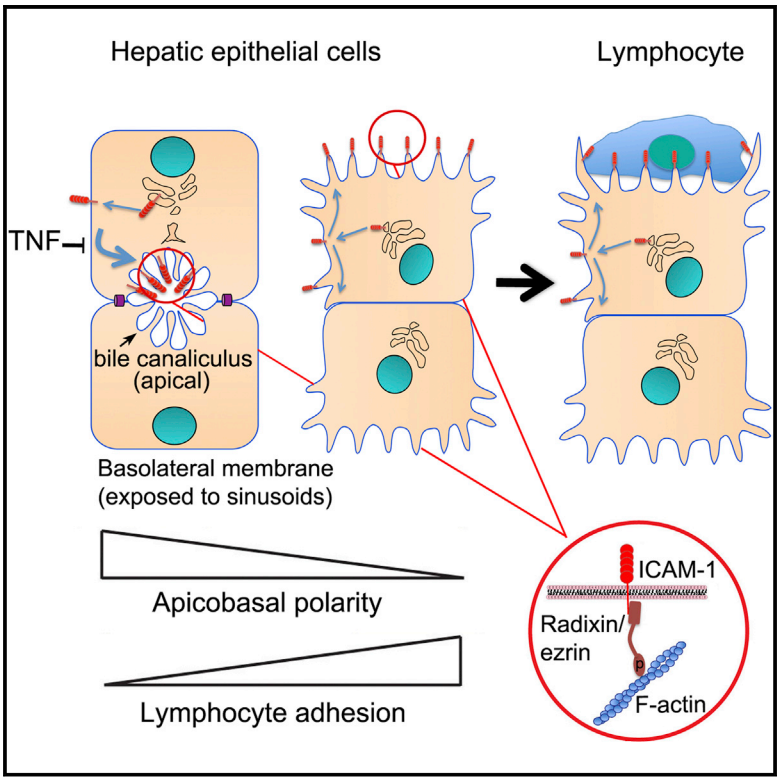

Highlights

Loss of apicobasal polarity increases lymphocyte adhesion to hepatic epithelial cells

The adhesion receptor ICAM-1 is apically confined in polarized hepatic cells

Upon loss of cell polarity, ICAM-1 is exposed and interacts with lymphocytes

Basolateral-to-apical transport prevents ICAM-1 basolateral localization

Authors

Natalia Reglero-Real, Adrián Álvarez-Varela, ..., Miguel A. Alonso, Jaime Millán

Correspondence

jmillan@cbm.csic.es

In Brief

Many epithelial pathologies induce loss of apicobasal polarity. Epithelial intercellular adhesion molecule 1 (ICAM-1) mediates lymphocyte adhesion to hepatic epithelial cells. Reglero-Real et al. now show that polarized hepatocytes and bile duct epithelial cells confine ICAM-1 to their apical membrane domains, which are less accessible to circulating immune cells. Upon depolarization, apical ICAM-1 is exposed and increases lymphocyte binding. Epithelial apicobasal polarity thus helps the immune system to discriminate between normal and depolarized, dysfunctional hepatic cells exposing their adhesion machinery.

Reglero-Real et al., 2014, Cell Reports 8, 1879–1893
September 25, 2014 ©2014 The Authors
http://dx.doi.org/10.1016/j.celrep.2014.08.007

Cell Reports
Article

Apicobasal Polarity Controls Lymphocyte Adhesion to Hepatic Epithelial Cells

Natalia Reglero-Real,[1] Adrián Álvarez-Varela,[1] Eva Cernuda-Morollón,[2] Jorge Feito,[3] Beatriz Marcos-Ramiro,[1] Laura Fernández-Martín,[1] Maria José Gómez-Lechón,[4,5] Jordi Muntané,[7] Pilar Sandoval,[1] Pedro L. Majano,[5,6] Isabel Correas,[1] Miguel A. Alonso,[1] and Jaime Millán[1,*]
[1]Centro de Biología Molecular Severo Ochoa. Consejo Superior de Investigaciones Científicas and Universidad Autónoma de Madrid, 28049 Madrid, Spain
[2]Facultad de Medicina, Universidad de Oviedo, 33006 Oviedo, Spain
[3]Servicio de Anatomía Patológica, Hospital Universitario Central de Asturias, 33006 Oviedo, Spain
[4]Unidad de Hepatología Experimental, Centro de Investigación, Hospital La Fe, 46026 Valencia, Spain
[5]Centro de Investigación Biomédica en Red para Enfermedades Hepáticas y Digestivas (CIBERehd), Instituto de Salud Carlos III, 28029 Madrid, Spain
[6]Unidad Biología Molecular, Hospital Universitario de la Princesa, Instituto de Investigación Sanitaria Princesa, 28006 Madrid, Spain
[7]Instituto de Biomedicina de Sevilla (IBiS) Hospital Universitario Virgen del Rocio/IBiS/CSIC/Universidad de Sevilla, 41013 Sevilla, Spain
*Correspondence: jmillan@cbm.csic.es
http://dx.doi.org/10.1016/j.celrep.2014.08.007

SUMMARY

Loss of apicobasal polarity is a hallmark of epithelial pathologies. Leukocyte infiltration and crosstalk with dysfunctional epithelial barriers are crucial for the inflammatory response. Here, we show that apicobasal architecture regulates the adhesion between hepatic epithelial cells and lymphocytes. Polarized hepatocytes and epithelium from bile ducts segregate the intercellular adhesion molecule 1 (ICAM-1) adhesion receptor onto their apical, microvilli-rich membranes, which are less accessible by circulating immune cells. Upon cell depolarization, hepatic ICAM-1 becomes exposed and increases lymphocyte binding. Polarized hepatic cells prevent ICAM-1 exposure to lymphocytes by redirecting basolateral ICAM-1 to apical domains. Loss of ICAM-1 polarity occurs in human inflammatory liver diseases and can be induced by the inflammatory cytokine tumor necrosis factor alpha (TNF-α). We propose that adhesion receptor polarization is a parenchymal immune checkpoint that allows functional epithelium to hamper leukocyte binding. This contributes to the haptotactic guidance of leukocytes toward neighboring damaged or chronically inflamed epithelial cells that expose their adhesion machinery.

INTRODUCTION

Hepatocytes are polarized epithelial cells that delimit an apical lumen that forms channels for draining bile, the bile canaliculi (BCs), and a basolateral membrane that is exposed to the space of Disse and interacts with the sinusoids, extravasated leukocytes, and other parenchymal cells (Lee, 2012; Wang and Boyer, 2004). BCs drain into bile ducts, which are formed by polarized epithelial cells called cholangiocytes (Lee, 2012). A correct polarized architecture is necessary for hepatic epithelial cell function, and loss of hepatic apicobasal polarity is a hallmark of liver pathology. Hepatocytes injured after trauma, hepatoma cells, and hepatocytes infected with hepatitis B virus (HBV) or hepatitis C virus (HCV) lose their polarity (Benedicto et al., 2011; Mee et al., 2010; Shousha et al., 2004). Reduced hepatocyte polarization has been found in biopsies of liver carcinomas and livers at different stages of cirrhosis or hepatitis infection (Shousha et al., 2004).

Leukocyte infiltration into the liver is essential for immune surveillance, controls cancer and infections, and facilitates tissue regeneration. Aberrant leukocyte-hepatocyte interactions trigger liver failure in autoimmune diseases and rejection after transplantation, and exacerbate liver damage upon severe trauma. Hepatocyte death, injury, oncogenic transformation, and virus infection promote extravasation across the sinusoids of immune cells, which search for antigen presentation, damaged or transformed cells, cell debris, or microorganisms (Hiraoka, 2010; Holz et al., 2010; Kang et al., 2011). Efficient leukocyte migration in the parenchyma involves various molecular cues, including secreted chemokines and cytokines, and haptotactic factors such as extracellular matrix components and adhesion receptors exposed on sinusoidal and parenchymal cell surfaces (Edwards et al., 2005; McGettrick et al., 2012). The interaction between leukocyte β2 integrins and intercellular adhesion molecule 1 (ICAM-1) is of central importance in the epithelial inflammatory response (Chin and Parkos, 2007). The molecular mechanisms that regulate leukocyte adhesion to hepatic epithelial cells have not yet been investigated in detail; however, a role for hepatic ICAM-1 as a counterreceptor of leukocyte integrins for neutrophils, T cells, and T cell hybridomas has been reported (Meijne et al., 1994; Morita et al., 1994; Nagendra et al., 1997).

Here we demonstrate that apicobasal polarity negatively regulates lymphocyte adhesion to hepatic cells through the

confinement of ICAM-1 in their apical membrane domains, which are not accessible by immune cells. This confinement is observed both in vitro and in vivo and is regulated by the proinflammatory cytokine tumor necrosis factor alpha (TNF-α). Our results indicate that in dysfunctional hepatic parenchyma, leukocytes appear to discriminate between operative hepatocytes that segregate adhesion receptors onto BCs and depolarized and chronically inflamed adjacent hepatocytes that expose their adhesion machinery.

RESULTS

Loss of Apicobasal Polarity Increases Lymphocyte Adhesion to HepG2 Cells

To investigate the effect of the loss of hepatocellular polarity on T lymphocyte adhesion, we first took advantage of the hepatoma cell line HepG2, which retains the main polarity features of primary hepatocytes and is thus a prototypical model for investigating apicobasal polarity (Madrid et al., 2010; van IJzendoorn et al., 1997). Depending on the cell passage, 40%–60% of HepG2 cells showed a polarized morphology, forming colonies containing spherical or tubular apical lumens between two or more cells (Figure 1A, left). These lumens are sealed by cell-cell junctions and are reminiscent of bona fide BCs (Madrid et al., 2010). It has been reported that classical PKC activation with phorbol esters, such as phorbol-12 myristate-13 acetate (PMA), reduces HepG2 polarization, whereas analogs of cyclic AMP (cAMP), such as dibutyryl-cAMP (dcAMP), promote the formation of BCs (Fu et al., 2011; Zegers and Hoekstra, 1997). We first analyzed the effect of PMA and dcAMP on HepG2 cell polarity and interaction with T lymphocytes. We addressed cell polarity by counting the number of BCs, as identified by double staining of F-actin and the glycosylphosphatidylinositol (GPI)-anchored protein CD59, which partially accumulates in the BCs (Figure 1A) or by double staining with the canalicular markers multidrug resistance-associated protein 2 (Mrp-2) and phosphorylated ezrin-radixin-moesin (ERM) proteins (Kikuchi et al., 2002; Figure S1). PMA reduced the number of BCs by 70% (Figure 1A) and the percentage of polarized cells to 10%–20% of total HepG2 cells. In contrast, dcAMP increased them by 23% respect to untreated cells. Interestingly, after extensive washes, PMA-treated HepG2 cells increased T cell adhesion by 71%, whereas dcAMP-treated HepG2 cells decreased it by 22% (Figure 1B). Signaling pathways that regulate cell polarity are involved in the inflammatory response (Mashukova et al., 2011) and can induce the expression of adhesion receptors that interact with immune cells (Delpino et al., 2010). To test whether the inverse correlation between apicobasal polarity and T cell adhesion could be attributed to the de novo synthesis of surface adhesion receptors, we performed depolarization assays in the presence of the inhibitor of protein biosynthesis cycloheximide (CHX). We observed no significant effect of CHX on polarity (not shown) or lymphocyte adhesion (Figure 1B) in either control or PMA-pretreated HepG2 cells, which indicates that this increase in T cell adhesion is independent of de novo receptor synthesis.

To rule out the possibility that PMA or dcAMP affect hepatic cell-leukocyte adhesion independently of the modulation of apicobasal polarity, we followed an alternative strategy and targeted the Cdc42-mediated signaling axis in HepG2 cells, which plays a central role in the generation of cell polarity. The Rho GTPase Cdc42 serves as a master regulator of cell polarity by controlling vesicular trafficking, cell-cell junctions, and signaling pathways that mediate cell polarization (Madrid et al., 2010; Martin-Belmonte et al., 2007). Cdc42 knockdown with two small interfering RNA (siRNA) oligonucleotides reduced the number of BCs in HepG2 cells to 52% and 53% of those found in cells transfected with siRNA control (Figures 1C and 1D). This reduction of polarity correlated with an increased adhesion of human primary T lymphocytes to hepatic cells by 35% and 27%, respectively (Figure 1E). Cdc42 regulates the partitioning-defective (PAR) polarity complex, which comprises the proteins PAR3, PAR6, and atypical protein kinase C (aPKC), and promotes the establishment of the apical-basal membrane border (Martin-Belmonte and Mostov, 2008). aPKC can be inhibited with a pseudosubstrate peptide (PS-aPKC) that impairs apical lumen morphogenesis (Martin-Belmonte et al., 2007). Similarly to Cdc42 knockdown, PS-aPKC reduced the number of BCs by almost 50% (Figure 1F) and increased lymphocyte adhesion by 62% (Figure 1G). Finally, in the absence of depolarizing treatment, we found that T lymphocytes preferentially adhered to the subpopulation of unpolarized hepatic cells (Figure 1H). In summary, by modulating the polarity of HepG2 cells using four different approaches, we identified an inverse correlation between their apicobasal architecture and their ability to interact with T lymphocytes.

ICAM-1 Is Confined in the BCs of Polarized Hepatocytes and Exposed to Lymphocytes upon Loss of Polarity

In the liver parenchyma, infiltrated leukocytes preferentially establish contacts with the basolateral membranes of polarized hepatic cells, which are exposed to the sinusoids (Warren et al., 2006). The β2 integrin counterreceptor ICAM-1 mediates leukocyte adhesion to endothelial and epithelial cells (Meijne et al., 1994; Reglero-Real et al., 2012). Confocal analysis of polarized HepG2 cells and human primary hepatocytes revealed low levels of ICAM-1 staining at basolateral membrane domains. The receptor was mostly confined to the BCs, where it colocalized with F-actin-rich microvilli (Figures 2A and 2B) and was surrounded by cell-to-cell junctional markers such as desmosomal desmoglein-2 (Dsg-2) (Figure S2A). The distribution of ICAM-1 was comparable to that of other canalicular markers, such as radixin, Mrp-2, and active phosphorylated ERM (p-ERM) proteins (ezrin [T567], radixin [T568], and moesin [T558] (Figure 2B; Kikuchi et al., 2002). Upon induction of HepG2 cell depolarization, canalicular ICAM-1 was dispersed in discrete domains distributed over the entire cell area (Figure 2C). These structures were positive for F-actin and resembled the staining pattern of ICAM-1-rich microvilli found in nonpolarized epithelial and endothelial cells (Figure 2C, inset; Millán et al., 2006). Phosphorylation at a specific threonine residue close to the C terminus is required to promote the open conformation of active ERMs (Ivetic and Ridley, 2004), which regulate microvilli by connecting F-actin to plasma membrane proteins. Untreated, polarized HepG2 cells accumulated active p-ERM proteins in the apical membranes (Figure 2D), as occurs in primary hepatocytes (Figure 2B; Kikuchi

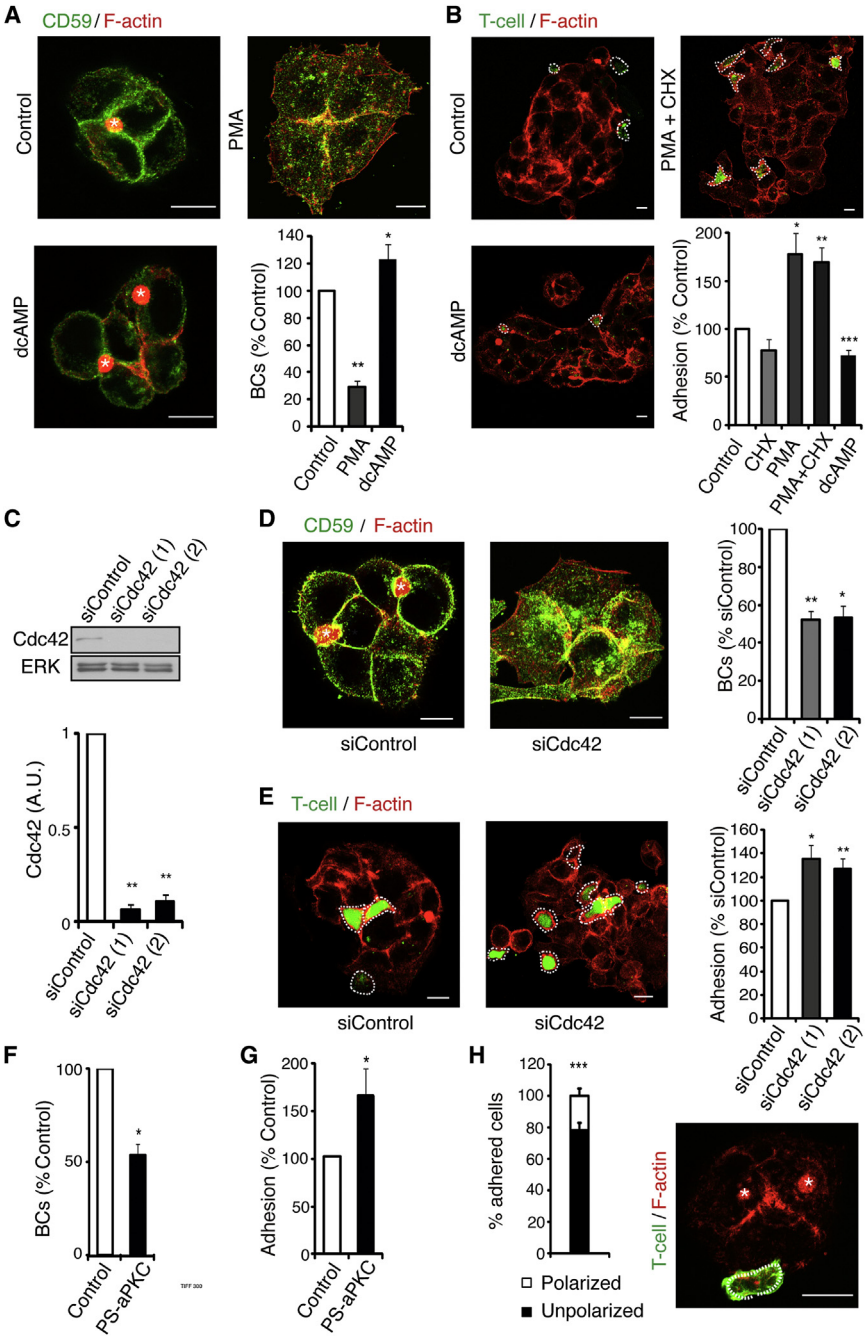

Figure 1. Epithelial Apicobasal Polarity Regulates T Lymphocyte Adhesion

(A) Confocal images of untreated HepG2 cells (Control) or cells treated for 2 hr with 100 nM PMA or with 100 μm dcAMP, fixed, and stained for CD59 and F-actin to identify apical membrane domains that form BCs (asterisks). The bottom-right graph shows the quantification of BCs. *p = 0.008; **p = 0.002; n = 3.

(B) HepG2 cells were treated as in (A). When indicated, protein biosynthesis was inhibited by coincubation with 1 μg/ml CHX. Cells were then extensively washed and incubated with calcein-labeled T lymphocytes for 15 min, rinsed, fixed, and stained for F-actin to visualize HepG2 and T cells. Discontinuous lines in confocal images mark calcein-positive T cells. Lymphocyte adhesion was quantified by measuring calcein fluorescence in a plate reader (bottom-right graph). *p = 0.008, n = 6; **p = 0.001, n = 8; ***p = 0.0007, n = 5.

(C) HepG2 cells were transfected with siRNA control (siControl) or two different siRNAs specific for Cdc42 (siCdc42) for 72 hr. Western blot of Cdc42 and ERK in siRNA-transfected cells. Bottom graph: quantification of Cdc42 levels expressed as arbitrary units (A.U.). ERK expression was used as a loading control. **$p < 2.8 \times 10^{-7}$; n = 3.

(D) Cells transfected with the indicated siRNAs were stained for F-actin and CD59 to identify (asterisks) and quantify (right graph) BCs. *p = 0.001; **p = 0.0003; n = 3.

(E) siRNA-transfected HepG2 cells were incubated with calcein-labeled T lymphocytes for 15 min, rinsed, fixed, and stained for F-actin. Lymphocyte adhesion was quantified as in (B) (bottom-right graph). *p = 0.031, n = 3; **p = 0.007, n = 5.

(F and G) Quantification of BCs (*p = 0.003) (F) and calcein-labeled T lymphocyte adhesion (*p = 0.043) (G) in untreated HepG2 cells (control) or HepG2 cells treated for 18 hr with 40 μg/ml of PS-aPKC.

(H) Untreated HepG2 cells were incubated with calcein-labeled T cells. The percentage of T cell adhesion to polarized versus unpolarized HepG2 cells is shown. ***p = 0.0005, n = 3. Bars show the mean + SEM. Scale bars represent 10 μm.

See also Figure S1.

et al., 2002). Upon collapse of the BCs, active ERMs were localized in sparse, discrete domains on the plasma membrane—a redistribution pattern that was very similar to that of microvilli and ICAM-1 (Figures 2C and 2D). Immunostaining of ICAM-1 prior to permeabilization of depolarized HepG2 cells stably expressing ICAM-1-GFP showed that ICAM-1 domains were exposed on the cell surface (Figure 2E). Scanning electron microscopy of HepG2 cells revealed the appearance of long surface filaments resembling canalicular microvilli upon induction of depolarization (Figure 2F). In order to analyze quantitatively whether plasma membrane ICAM-1 is more exposed to the extracellular milieu upon depolarization, we labeled surface proteins of untreated or depolarized HepG2 cells in the cold with membrane-impermeable sulfo-NHS-biotin, which could not reach the BCs. Biotinylated (and thus exposed) ICAM-1 was detected by pull-down assays with neutravidin-conjugated agarose (Figure 2G). Although not all of the untreated HepG2 cells had a polarized phenotype before the induction of depolarization, the exposed-to-total protein ratio clearly showed that ICAM-1 and p-ERM proteins, which were associated with biotinylated plasma membrane receptors, were more accessible from the extracellular milieu in response to the depolarizing

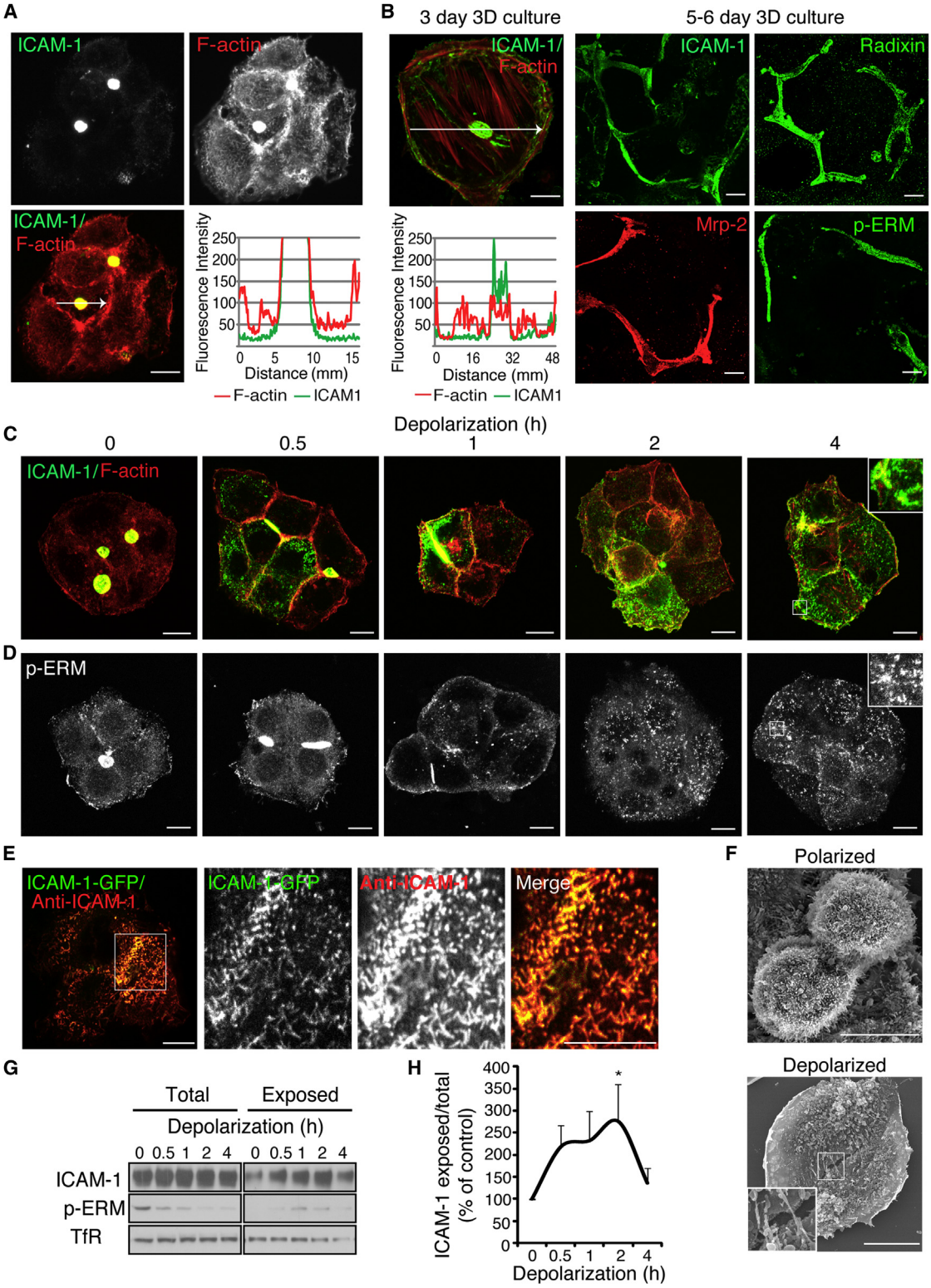

Figure 2. ICAM-1 Is Confined in BCs of Human Hepatocytes and Exposed upon Loss of Apicobasal Polarity

(A) HepG2 cells were grown for 72 hr, fixed, and stained for ICAM-1 and F-actin. The bottom right shows the fluorescence intensity profile along the white arrow crossing a BC in the image.

(legend continued on next page)

challenge. Cdc42 knockdown and incubation with PS-aPKC also increased ICAM-1 dispersion (Figure S2B) and biotinylation (Figure S2C). Altogether, these findings indicate that loss of polarity exposes actin- and ERM-rich canalicular microvilli containing ICAM-1 on cell surfaces.

Indeed, time-lapse analysis of T cells migrating on depolarized HepG2 stably expressing ICAM-1-GFP showed local receptor redistribution into microvilli-like protrusions surrounding the adhered lymphocyte (Figure 3A, arrows; Movie S1). Extensive confocal analysis followed by 3D image reconstruction also revealed endogenous ICAM-1- and F-actin-rich membrane projections around lymphocytes adhered to unpolarized hepatic cells (Figures 3B–3D). This membrane reorganization resembles the endothelial docking structures that mediate leukocyte transendothelial migration (TEM) (Barreiro et al., 2002; van Buul et al., 2007). Finally, we tested whether ICAM-1 mediates lymphocyte adhesion in depolarized HepG2 cells. HepG2 cells were transfected with control siRNA or two different siRNA oligonucleotides that efficiently knock down ICAM-1 (siICAM-1) (Figure 3E). Cells were then depolarized with PMA+CHX and T cell adhesion assays were performed. ICAM-1-depleted hepatic cells showed a significant reduction in T cell adhesion, which was ~50% of the increase in adhesion observed upon induction of depolarization (Figures 3F and 1B). As a control, transfection of siICAM-1(2), which targets the 5′ UTR of ICAM-1 mRNA, did not reduce ICAM-1-GFP expression (Figure 3E) and thus had no effect on lymphocyte adhesion to HepG2 cells expressing exogenous ICAM-1 (Figure 3F). These results imply that the effect of ICAM-1 siRNA specifically results from a reduction in endogenous ICAM-1 expression. Consistent with these findings, blocking antibodies against ICAM-1 or LFA-1 also reduced lymphocyte adhesion to HepG2 cells (Figure 3G).

Polarized Hepatic Cells Prevent ICAM-1 Exposure to Basolateral Membranes by Redirecting Basolateral ICAM-1 to BCs

To investigate the mechanisms whereby polarized cells prevent ICAM-1 localization at basolateral domains that face circulating immune cells, we first studied the dynamics of polarized ICAM-1. ICAM-1 fused from its cytoplasmic C terminus to a photoactivatable GFP (paGFP) protein was generated and stably expressed in HepG2 cells (Patterson and Lippincott-Schwartz, 2002). Like endogenous ICAM-1 (Figure 2A) and ICAM-1-GFP (see Figure 5B), ICAM-1-paGFP was confined to the canalicular membrane of polarized HepG2 cells (not shown). To identify polarized cell colonies, actin-cherry was expressed in ICAM-1-paGFP-HepG2 cells. ICAM-1-paGFP was first photoactivated in the BCs and examined by time-lapse confocal microscopy (Figures 4A and 4B; Movie S2). No significant decrease in fluorescence was detected during the first 100 min poststimulation. The increase in fluorescence in the adjacent basolateral regions was also negligible, implying that ICAM-1-paGFP is remarkably confined in BCs. Intracanalicular diffusion could not be adequately analyzed due to the small size of these structures. Polarized targeting to the canalicular surface of newly synthesized proteins can take place by direct and indirect transport routes. In the direct route, proteins from the Golgi are delivered directly to the apical membrane. However, some apical proteins, including a number of single-span transmembrane proteins, can follow an indirect pathway and be segregated in the Golgi into different carriers that transport them first to the basolateral membrane and then to their final apical destination by transcytosis (Bastaki et al., 2002). Similar to what was observed for endogenous ICAM-1, only a minor fraction of ICAM-1-paGFP was localized at the basolateral membrane domains. Importantly, this fraction could be photoactivated, although it yielded much less intense fluorescence (Figure 4C; Movie S3). Compared with the slow apical-to-basolateral diffusion rate, ICAM-1-paGFP completely diffused out from basolaterally photoactivated areas within the first 10 min following photoactivation (Figures 4C and 4D; Movie S3). Long-term analysis of basolaterally photoactivated ICAM-1-paGFP revealed that the receptor first diffused within basolateral membranes and then accumulated progressively in the BCs. Simultaneously, basolateral fluorescence decreased, indicating the existence of a basolateral-to-apical trafficking of ICAM-1 (Figures 4E and 4F; Movie S4). Therefore, this population of basolaterally delivered ICAM-1 undergoes subsequent redirection to the apical canaliculus in polarized hepatic cells, where it can remain stable for at least 100 min. Consistent with these results, although only a minor fraction of ICAM-1 was localized in the basolateral membrane, basolateral ICAM-1 (not shown) and ICAM-1-GFP (Figure 4G) could be clearly labeled in live, unpermeabilized cells with a specific antibody. At 90 min after this immunolabeling, the antibody partially accumulated in BCs, indicating a basolateral-to-apical transport of labeled ICAM-1. Hence, these results indicate that the

(B) Primary human hepatocytes were grown for 3 days in collagen sandwiches and then fixed and stained for ICAM-1 and F-actin (top left). The bottom left shows the fluorescence intensity profile along the white arrow crossing a BC. Primary human hepatocytes were grown for 5–6 days in collagen sandwiches, fixed, and stained for ICAM-1, radixin, Mrp-2, or p-ERM proteins (right).

(C and D) HepG2 cells grown for 72 hr were depolarized with PMA+CHX for the indicated times. Cell were fixed and stained for F-actin and ICAM-1 (C) or for p-ERM proteins (D).

(E) HepG2 cells stably expressing ICAM-1GFP were depolarized as in (C) for 2 hr, incubated in the cold with anti-ICAM-1 antibody, fixed, and analyzed by confocal microscopy.

(F) Scanning electron microscopy analysis of polarized and depolarized HepG2 cells. The enlarged area shows microvilli-like protrusions appearing in cells that are losing their polarity.

(G) HepG2 cells undergoing depolarization by PMA+CHX treatment at different times were incubated with sulfo-NHS-biotin and lysed. Surface-biotinylated proteins (Exposed) were isolated by pull-down assay with neutravidin-agarose.

(H) The ratio of extracellularly exposed-to-total ICAM-1 is expressed as a percentage of the ratio in control cells. Surface ICAM-1 levels increased between 2- and 3-fold upon loss of polarity and subsequently decayed at later times due to the constitutive internalization of surface proteins in CHX-treated cells. *$p = 0.034$, $n = 4$. Scale bars represent 10 μm.

See also Figure S2.

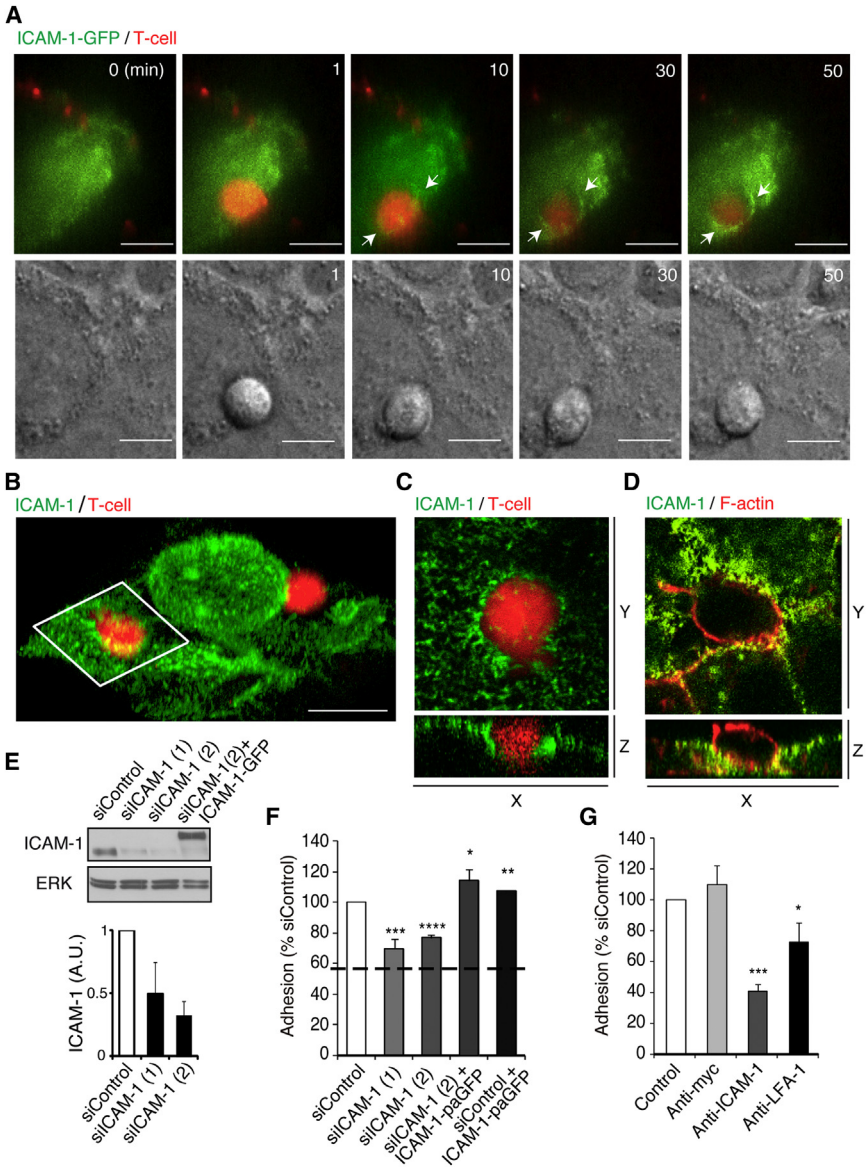

Figure 3. ICAM-1 Mediates T Cell Adhesion to Depolarized Hepatic Epithelial Cells

(A) Depolarized HepG2 cells expressing ICAM-1-GFP were incubated with CMTMR-labeled T lymphocytes and analyzed by time-lapse fluorescence microscopy and phase contrast. Arrows indicate the accumulation of ICAM-1-GFP around one adhered T lymphocyte.

(B) A z stack reconstruction of confocal images of hepatic ICAM-1 surrounding adhered T lymphocytes labeled with CMTMR.

(C) Maximum intensity projection of the boxed area in (B). The three orthogonal axes are indicated.

(D) Maximum intensity projection of confocal z-stacks of ICAM-1 and F-actin staining of a T cell adhered to depolarized HepG2 cells. The three orthogonal axes are indicated.

(E) Control HepG2 cells or HepG2 cells stably expressing ICAM-1-GFP were transfected with the indicated siRNA oligonucleotides. After 72 hr, cells were lysed and immunoblotted for the indicated proteins. Exogenous ICAM-1 was not depleted by siICAM-1(2). The bottom histogram quantifies ICAM-1 levels in siICAM-1 transfected cells relative to siControl cells in arbitrary units (A.U.).

(F) Effect of the indicated siRNAs on T lymphocyte adhesion to depolarized control HepG2 cells or HepG2 cells stably expressing ICAM-1-paGFP, a photoactivatable form of GFP that yields no fluorescence in the plate reader. The discontinuous line shows the percentage of T cell adhesion levels in untreated and polarized HepG2 cells. *$p = 0.041$, $n = 5$; **$p = 0.004$, $n = 3$; ***$p = 0.0004$, $n = 5$; ****$p = 5.3 \times 10^{-5}$, $n = 6$.

(G) T lymphocyte adhesion assays to depolarized HepG2 cells were performed in the presence of the indicated blocking antibodies. *$p = 0.044$, $n = 3$; ***$p = 3.618 \times 10^{-7}$, $n = 5$. Bars show the mean + SEM. Scale bars represent 10 μm.

See also Movie S1.

substantive differences between basolateral-to-apical and apical-to-basolateral trafficking of surface ICAM-1 prevent receptor localization at basolateral membranes, which in vivo are exposed in the liver to the space of Disse, vasculature, and immune cells.

ICAM-1 Associates with ERM Proteins at the Plasma Membrane through Its Cytoplasmic Tail, which Is Required for ICAM-1 Apical Localization

We next addressed which receptor domain is responsible for ICAM-1 confinement in BCs. Basolateral localization of ICAM-1-Δct-GFP, which lacks the receptor cytoplasmic tail, was increased compared with the ICAM-1-GFP distribution, whereas GFP fused to ICAM-1 lacking the extracellular domain (GFP-ICAM-1-Δext) was sufficient to target GFP to BCs (Figures 5A–5D). These results indicate that apical segregation of ICAM-1 is partially dependent on its cytoplasmic segment. To gain insight into the role of the ICAM-1 cytoplasmic segment in ICAM-1 polarity, we stably expressed ICAM-1-Δct-paGFP in hepatic cells and analyzed its dynamics after photoactivation. Absence of the cytoplasmic segment did not reduce the canalicular confinement of ICAM-1-Δct-paGFP (Figures 5E and S3A; Movie S5). In contrast, basolateral-to-apical trafficking was clearly reduced compared with that of ICAM-1-paGFP (Figures 5F, S3B, and S3C; Movie S6), suggesting that the ICAM-1 cytoplasmic segment regulates the basolateral-to-apical traffic of ICAM-1. Adhesion receptors from the immunoglobulin superfamily, such as ICAM-1 and VCAM-1, can interact from their cytoplasmic tail with proteins that connect them to the subcortical actin cytoskeleton, such as filamin, α-actinin, and the ERM proteins (Barreiro et al., 2002; Carpén et al., 1992; Kanters et al., 2008; Oh et al., 2007). Radixin and ezrin, which are the most abundant ERM proteins in hepatocytes and hepatoma cells, are essential for maintaining the BC structure and determine the

apical localization of canalicular membrane proteins such as Mrp-2 (Gilbert et al., 2012; Kikuchi et al., 2002). We found that ICAM-1 colocalized with radixin and ezrin in polarized and depolarized cells (Figure 5G). Furthermore, antibody-mediated crosslinking of ICAM-1 induced radixin-YFP and ezrin-GFP coclustering at the plasma membrane in HepG2 cells (Figure 5H). ICAM-1 crosslinking in primary human hepatocytes induced a significant coclustering of active ERM proteins (Figure S3D). This coclustering depended on the receptor cytoplasmic segment, since ICAM-1 Δct-GFP clusters accumulated significantly fewer p-ERM proteins at the plasma membrane of HepG2 cells compared with ICAM-1-GFP clusters (Figure 5I). In accordance with this, pull-down assays revealed that the ICAM-1 cytoplasmic tail associates with phosphorylated radixin and ezrin (Figure 5J). The substitution of three lysine residues close to the transmembrane segment of the receptor by leucine was sufficient to abrogate the binding of hepatic ERM proteins to the receptor cytoplasmic segment (Figures 5J and 5K) and induced a partial depolarization of ICAM-1 (Figure 5L). This supports previous reports describing the requirement of a short domain that contains basic amino acids for the interaction between the ICAM-1 tail and actin connectors in other cell types (Carpén et al., 1992; Oh et al., 2007). ICAM-1-K>L-GFP was not as depolarized as ICAM-1-Δct-GFP, which suggests that additional interactions of ICAM-1 tail with other cytoplasmic proteins contribute to the receptor polarity. Collectively, these results indicate that in hepatic cells, ICAM-1 is also associated with active ERM and F-actin in microvilli, a machinery that mediates leukocyte adhesion when exposed to leukocytes (Reglero-Real et al., 2012) and also plays an important role in the maintenance of apicobasal polarity (Kikuchi et al., 2002; Wang et al., 2006).

Long-Term TNF-α Stimulation Activates ERM Proteins at Basolateral Domains and Increases ICAM-1 Basolateral Exposure

ICAM-1 expression, ERM protein activation, and leukocyte adhesion are induced by the cytokine TNF-α (Aranda et al., 2013; Koss et al., 2006), which is fundamental to long-term liver inflammatory responses. We investigated the effect of long-term stimulation by TNF-α on hepatocellular polarity and ICAM-1 expression and polarization. HepG2 cells were stimulated at different times and the distribution of ICAM-1 was analyzed. In conjunction with a clear effect on ICAM-1 expression, immunofluorescence and surface biotinylation assays revealed that TNF-α significantly increased ICAM-1 and ICAM-1-GFP exposure to the extracellular milieu (Figures 6A and 6B). Importantly, 24 hr of TNF-α stimulation did not change the number of BCs in HepG2 cultures (Figure 6C) or the distribution of the cell-to-cell junctional marker ZO-1 (Figure S4A), which suggests that the increase of ICAM-1 basolateral localization is not a consequence of TNF-α-mediated loss of apicobasal polarity. The analysis of TNF-α-induced ICAM-1 depolarization in the presence of CHX revealed that de novo synthesis of ICAM-1 is required for its basolateral localization (Figure S4B), suggesting that newly synthesized ICAM-1 reaches the basolateral domains first. Interestingly, TNF-α had no effect on the apical confinement of ICAM-1 (Figure S4C; Movie S7), but significantly reduced the basolateral-to-apical trafficking of the receptor (Figures 6D and S4D).

TNF-α induced ERM phosphorylation in membrane protrusions at the basolateral membrane, which resembled surface microvilli (Figure 6E). An overall increase in ERM phosphorylation was also detected by western blot analysis, which showed that this increment occurred before the increase in ICAM-1 (Figure 6F). ICAM-1 knockdown had no effect on ERM phosphorylation (not shown), ruling out a role for the receptor itself in ERM activation. For correct function and localization, ERM proteins must cycle between their active and inactive conformations (Viswanatha et al., 2012). A constitutively active ERM mutant, ezrin T567D GFP (ezrin-TD-GFP), was mislocalized to the basolateral membrane. The expression of ezrin-TD-GFP was sufficient to induce the basolateral accumulation of ICAM-1 in HepG2 cells (Figure 6G) and to reduce basolateral-to-apical trafficking of ICAM-1 in cells with morphologically intact BCs (Figures 6H and S4E), similar to the reduction observed upon long-term TNF- stimulation (Figures 6D and S4D). Expression of GFP alone had no effect on ICAM-1 polarization (Figure S4F). Together, these data indicate that basolateral ERM activation in response to long-term TNF-α activation can contribute to basolateral exposure of ICAM-1 without affecting the integrity of BCs in hepatic cells. The basolateral increase of ICAM-1 occurs by the delivery of newly synthesized ICAM-1 to the basolateral membrane and the subsequent slowdown of its basolateral-to-apical transport. ERM protein loss-of-function experiments were shown to affect overall hepatic cell polarization (Suda et al., 2011; Wang et al., 2006), which prevented these strategies from being adopted for further studies of ICAM-1 distribution.

Polarized Hepatocytes and Bile Duct Epithelial Cells Can Confine ICAM-1 to the Apical Membrane Domains

Finally, we studied ICAM-1 distribution in human tissue samples from healthy donors and from patients with short-term or chronic inflammatory liver dysfunction (Tables S1 and S2). First, we analyzed samples from rejected human liver allografts that were collected after a relatively short inflammatory response by the host, which preserved their hepatocyte integrity in many tissue areas. ICAM-1 was detected in the endothelial cells lining the sinusoids, but also in hepatocytes that were concentrated in BCs in areas that were apparently undamaged and showed no leukocyte infiltration (Figure S5A, images R1–R3, arrows, right insets). ICAM-1 expression was also significant in the sinusoids from healthy control donors, but it was weak or absent in most of the hepatocytes (Figure S5A, image Ct, arrows). Epithelial cells from some bile ducts also expressed ICAM-1, always polarized in the apical surface (Figure S5B). Hepatocytes expressing polarized ICAM-1 were often found close to portal areas, whereas small foci of parenchymal cells expressing depolarized ICAM-1 were occasionally found dispersed in the parenchyma (Figure S5C). Given that periportal hepatocytes are in proximity to T cell infiltrates, ICAM-1 polarization may constitute a protective mechanism for healthy hepatocytes that potentially can be exposed to immune cells. In contrast, in the parenchyma from livers in advanced stages of HCV and HBV infection, we found ICAM-1 confinement in BCs in some areas, but also a remarkable loss of ICAM-1 polarization in others. Immunohistochemical analysis of consecutive tissue sections, followed by accurate pattern recognition based on duct, sinusoidal, and canalicular

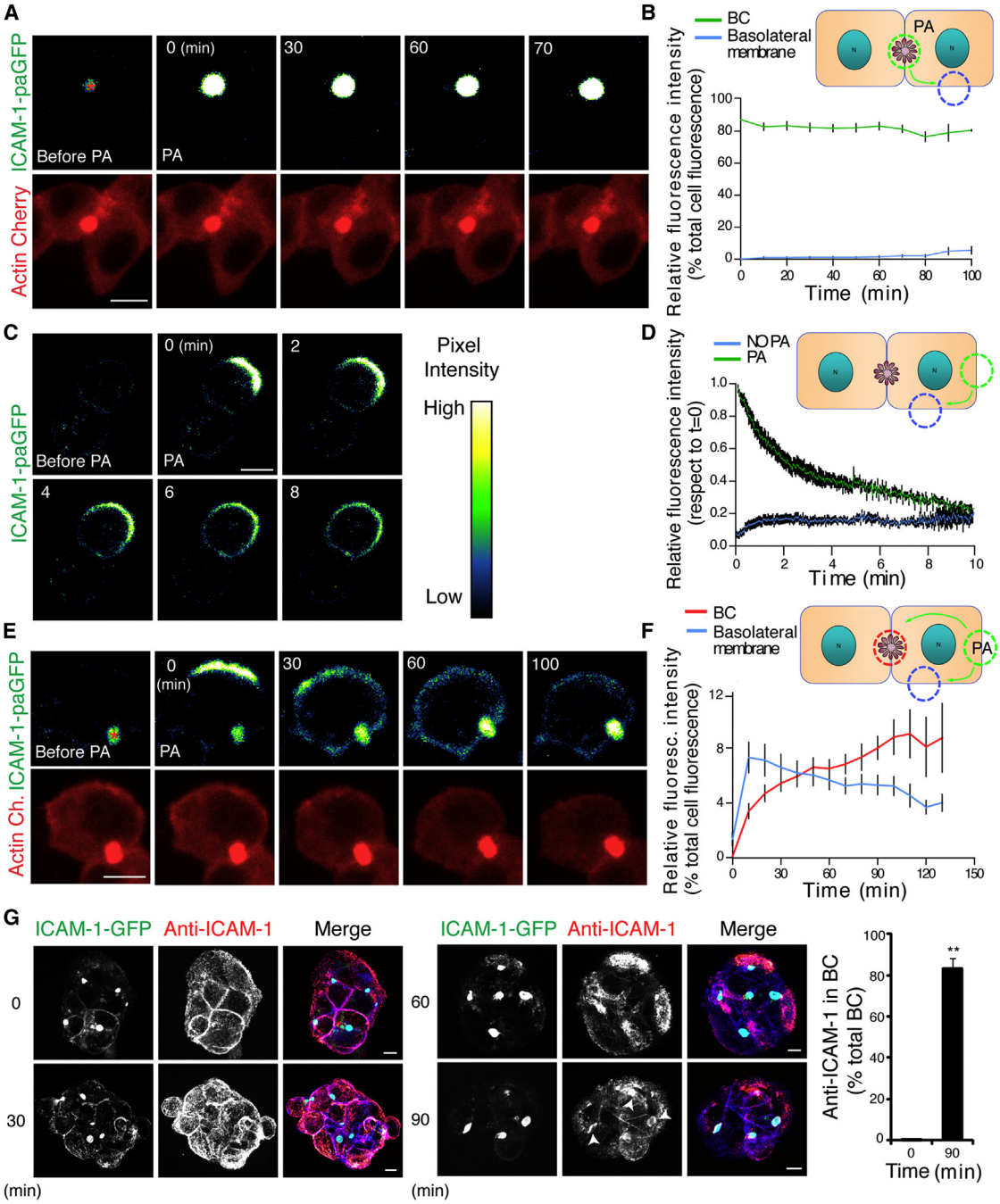

Figure 4. Basolateral ICAM-1 Is Redirected to and Confined in the BCs in Polarized HepG2 Cells

(A–F) ICAM-1 tagged with photoactivatable GFP (ICAM-1-paGFP) was photoactivated at the canalicular (apical) membrane (A and B) or the basolateral membrane (C–F) of polarized HepG2 cells.

(A) Apically photoactivated ICAM-1-paGFP is confined in the BC. Cells were previously transfected with actin-Cherry to visualize BCs. Canalicular ICAM-1 was photoactivated and its dynamics was analyzed by time-lapse confocal microscopy for more than 100 min. The asterisk marks the background fluorescence emission prior to photoactivation (PA).

(B) Quantification of the relative fluorescence intensity in photoactivated canalicular areas (BC) and adjacent basolateral membrane regions after background subtraction (n = 13 cells).

(C and D) Basolateral ICAM-1-paGFP was photoactivated and its dynamics was analyzed by time-lapse confocal microscopy for 10 min.

(D) Quantification of the relative fluorescence intensity in photoactivated and nonphotoactivated adjacent areas after background subtraction (n = 18 cells).

(E and F) Canalicular accumulation of basolaterally photoactivated ICAM-1. Basolateral ICAM-1-paGFP was photoactivated and its dynamics was analyzed by time-lapse confocal microscopy for 100 min. Basolateral ICAM-1-paGFP rapidly diffused along the adjacent membrane regions as in (A). At later times,

(legend continued on next page)

distribution, revealed a good correlation between the hepatic accumulation of ICAM-1 and the CD10 canalicular marker in some regions (Figures 7A and 7B). Similar to what was observed in sections from allograft rejections, cholangiocytes from some bile ducts strongly expressed and polarized ICAM-1 in luminal membrane domains (Figure 7B). As previously reported (Shousha et al., 2004), hepatocytes in many tissue regions lost apicobasal polarity and as a consequence also displayed an unpolarized ICAM-1 distribution (Figure 7C). However, a significant number of hepatocytes that did not apparently polarize ICAM-1 still concentrated CD10 into canalicular-like structures (Figure 7D), suggesting the existence in vivo of mechanisms that induce ICAM-1 basolateral exposure in polarized hepatocytes, such as strong stimulation by inflammatory cytokines. Taken together, these data reveal that hepatic parenchymal cells with an intact apicobasal architecture can segregate the ICAM-1 receptor onto apical surfaces, which may not be accessible from sinusoidal or perisinusoidal cells such as infiltrated leukocytes. ICAM-1 loses its apical polarity in chronic liver diseases that affect the hepatocyte architecture and cause persistent inflammatory stress.

DISCUSSION

Immunosurveillance plays a central role in clearing and receiving information from dysfunctional epithelial cells in the parenchyma (Chin and Parkos, 2007; Kang et al., 2011). However, the molecular mechanisms that regulate the communication between immune cells and the hepatic epithelium are still poorly understood. ICAM-1 contributes to leukocyte adhesion to primary, nonpolarized hepatocytes (Meijne et al., 1994; Morita et al., 1994) and to hepatocyte-derived cell lines stimulated with a proinflammatory cytokine cocktail (Nagendra et al., 1997). Here we show that unstimulated cultured HepG2 and primary hepatocytes, as well as hepatocytes from undamaged hepatic parenchymal regions, remarkably segregate ICAM-1 into apical plasma membranes. Hepatic cells must lose polarity or be exposed to long-term inflammatory stimulation in order to make this receptor accessible to immune cells. Hence, the polarized architecture of hepatic cells emerges as a mechanism for modulating the intensity of the inflammatory response in the liver. Recent reports indicated that hepatocytes play a more important role in leukocyte adhesion than expected, even before immune cells egress from the hepatic microcirculatory system, since ICAM-1 on hepatocyte microvilli directly contact leukocytes circulating by the sinusoids through endothelial fenestrae (Warren et al., 2006). In this way, ICAM-1 participates in antigen presentation to circulating, sinusoidal lymphocytes, which may be a determinant in the pathogenesis of viral hepatitis or in liver-induced immune tolerance. Thus, hepatic ICAM-1 polarization may be relevant for both innate and adaptive immune responses in the liver.

In hepatic cells exposing ICAM-1 upon depolarization, the receptor is reorganized into microvilli-derived structures that embrace interacting lymphocytes. These structures are similar to the docking complexes formed between ICAM-1 and ERM proteins in endothelial cells, which are required for an efficient leukocyte TEM (Barreiro et al., 2002; Reglero-Real et al., 2012). However, in hepatocytes, active ERM proteins play roles other than those described for leukocyte extravasation. The luminal domain of hepatocytes delimits the BC, a channel in which microvilli are abundant and the hepatocytes drain bile. Subcortical filamentous actin and ERM proteins accumulate in BCs and regulate cell polarity, canalicular microvilli, and canalicular membrane localization of proteins such as the detoxifying transporter Mrp-2 (Kikuchi et al., 2002; Wang et al., 2006). Our data suggest that the ERM protein's interaction with hepatic ICAM-1 also plays a role in its polarized localization, which in turn determines the lymphocyte-hepatic cell interaction. We propose that the dual role of the protein machinery formed by ERM proteins and microvillar actin bundles (i.e., regulating either lymphocyte adhesion or apicobasal polarity) underlies the inverse relation found between these two processes in hepatic cells. When confined in canalicular microvilli, the machinery regulates hepatocellular polarity and drainage functions while it also contributes to attenuate the inflammatory response by confining adhesion receptors. Upon cell damage or persistent inflammation with cytokines such as TNF-α, the machinery is exposed and plays haptotactic roles comparable to those observed in endothelial cells.

Using different experimental strategies, we have also demonstrated that the basolateral-to-apical traffic of ICAM-1 regulates its polarity. The basolateral activation of ERM proteins by TNF-α delays basolateral-to-apical trafficking of ICAM-1, probably by retaining the receptor associated with basolateral actin structures (Oh et al., 2007). Further studies on the mechanisms that regulate the activation of ERM proteins in different membrane domains in hepatic cells may thus facilitate the development of new therapeutic approaches to control the distribution of adhesion receptors and liver function during inflammation.

Collectively, our data obtained in vitro indicate that in addition to chemotactic gradients, hepatocellular polarity and the extension of the inflammatory response may provide haptotactic cues that infiltrated leukocytes use to discriminate dysfunctional hepatocytes from polarized, still-operative hepatocytes in damaged parenchyma. Of note, the ICAM-1 distribution observed in human tissue samples from livers with acute or long-term inflammatory dysfunction is consistent with our in vitro observations. Liver allograft rejections and livers chronically infected with

fluorescence decreased from the basolateral regions and accumulated in the canalicular areas. The asterisk marks the background fluorescence emission detected prior to PA.

(F) Quantification of fluorescence in basolateral and canalicular (BC) regions adjacent to photoactivated areas after background subtraction (n = 17 cells).

(G) Basolateral ICAM-1 was labeled with anti-ICAM-1 antibody in polarized HepG2 cells stably expressing ICAM-1-GFP. At the indicated times, cells were fixed, permeabilized, and stained with TRITC-conjugated secondary antibody. Basolaterally labeled ICAM-1 receptor was partially found in BCs 90 min after antibody incubation (arrowheads). Right graph: quantification of the percentage of BCs that were positive for basolateral ICAM-1. $^{**}p = 0.0002$, n = 4. Bars show the mean + SEM. Scale bars represent 10 μm.

See also Figure S3 and Movies S2, S3, and S4.

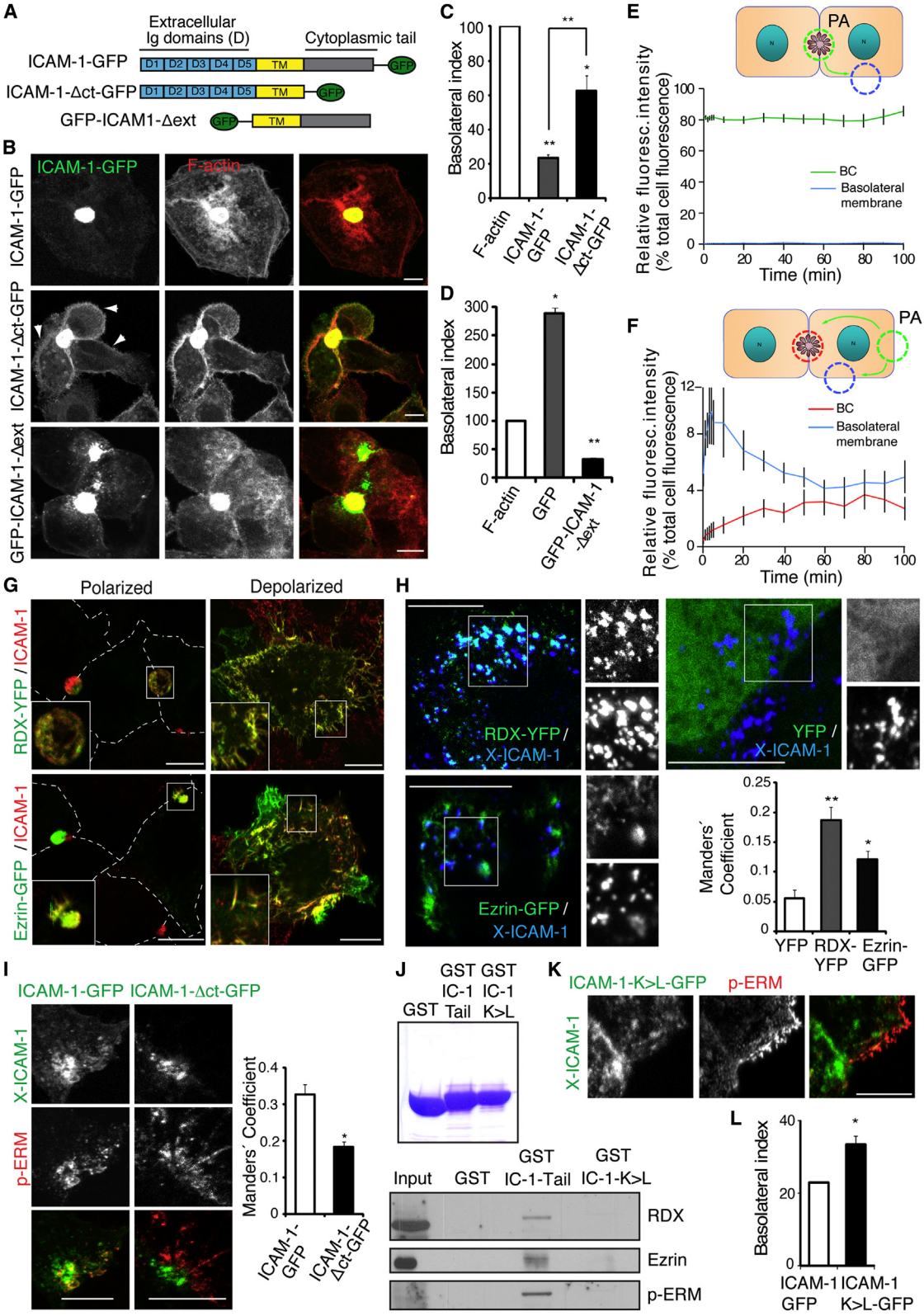

(legend on next page)

HBV and HCV accumulated ICAM-1 in BCs in areas that preserved hepatocyte integrity. However, the hepatitis virus-infected livers clearly contained extensive parenchymal regions that lost hepatic apicobasal polarity, as revealed by staining of the canalicular marker CD10. They also had areas in which ICAM-1 had an unpolarized distribution but CD10 was still concentrated in canalicular-like structures, which is consistent with the existence of a persistent inflammatory response that promotes receptor basolateral accumulation in correctly polarized hepatocytes. Several inflammatory and stress stimuli contribute to ICAM-1 expression (Hubbard and Rothlein, 2000; Morita et al., 1994; Zhu et al., 2005). Elucidating which stimulus regulates ICAM-1 polarization in hepatic cells in each pathological scenario is a long-term task that may provide a new perspective on the control of liver inflammatory diseases.

Our data are in agreement with those of a previous study of HBV-infected livers, in which parenchyma with mild HBV infection accumulated ICAM-1 in BCs, whereas parenchyma with high levels of LFA-1-positive lymphocyte infiltration and an exacerbated inflammatory response displayed a nonpolarized distribution of hepatocyte ICAM-1 (Doi et al., 1994). Although no analysis of hepatocyte polarity was carried out in that particular report, other researchers have shown that HCV and HBV liver infections reduce hepatocyte polarity and contribute to the development of a hepatocellular-transformed phenotype (Akkari et al., 2012; Kew, 2011; Wilson et al., 2012). Considering all these data together, we envisage that ICAM-1 basolateral exposure may help immune cells to identify hepatocytes in advanced stages of virus infection.

Mechanisms of apicobasal polarity are preserved in different epithelia, where the accessibility of immune cells to the lumens and internal cavities may be reduced relative to that in parenchymal spaces (Weisz and Rodriguez-Boulan, 2009). Therefore, polarization of epithelial receptors involved in adhesion and activation of immune cells may be a general mechanism to prevent exacerbation of the immune response that is not restricted to hepatic tissues. Indeed, an apical distribution of ICAM-1 has also been reported in human intestinal epithelia, in which this receptor mediates apical-to-basolateral leukocyte transmigration (Parkos et al., 1996). Since loss of polarity is a general feature of epithelial cell dysfunction, we propose that the differential exposure of adhesion receptors that occurs as a consequence is an immune checkpoint for maintaining epithelial tissues free of damaged or transformed cells.

EXPERIMENTAL PROCEDURES

Cells

Human hepatoma HepG2 cells were grown in high-glucose Dulbecco's modified Eagle's medium supplemented with 5% fetal bovine serum (Sigma). For stable expression of exogenous proteins, transfected cells were selected by treatment with 0.5 mg/ml G-418 sulfate for at least 4 weeks after transfection. Positive cell clones were maintained in drug-free medium. After several passages in this medium, >90% of cells retained expression of the exogenous product. Primary human hepatocytes were grown in collagen sandwiches with HCM medium (Lonza) for 5 days to induce polarization as previously described (Tolosa et al., 2011). T lymphoblasts were prepared from isolated human peripheral blood mononuclear cells (PBMCs). Nonadherent PBMCs were stimulated with 0.5% phytohemagglutinin for 48 hr and maintained in interleukin-2 as previously described (Millán et al., 2006). T lymphoblasts were used in experiments after they were cultured for 7–12 days.

Modulation of HepG2 Polarity

In addition to Cdc42 siRNA transfection, HepG2 cell polarity was reduced by treatment with 100 nM PMA for up to 4 hr (Zegers and Hoekstra, 1997) or with 40 μg/ml PS-aPKC for 18 hr. Polarity was increased by treatment with 100 μM dcAMP for 2 hr as previously described (Zegers and Hoekstra, 1997). Morphological analyses and BC quantitation were performed by staining for F-actin and CD59 in fixed HepG2 cells or primary hepatocytes.

Figure 5. ICAM-1 Apical Polarization and Association with Hepatic Radixin and Ezrin Require an Intact Receptor Cytoplasmic Tail

(A–D) The ICAM-1 cytoplasmic tail is required for full ICAM-1 apical polarization.

(A) Schematic of full and truncated ICAM-1 chimeras ectopically expressed in polarized HepG2 cells.

(B) HepG2 cells stably expressing ICAM-1-GFP and ICAM-1-Δct-GFP were grown for 72 hr and then fixed and stained for F-actin. Long-term expression of GFP-ICAM-1-Δext was toxic, so this chimera could only be transiently expressed. Intracellular accumulation of the protein was also detected.

(C and D) Quantification of the basolateral-to-apical ratio (basolateral index) of the indicated proteins normalized to the F-actin basolateral index. ICAM-1-Δct-GFP increased basolateral distribution, whereas the receptor transmembrane and tail domains were sufficient to localize GFP in the BC. (C) *p = 0.007, **p = 9×10^{-7}, n = 3. (D) *p = 2.2×10^{-5}, **p = 6.4×10^{-6}, n = 3.

(E) Apically photoactivated ICAM-1-Δct-paGFP is confined in the BC. Canalicular ICAM-1 was photoactivated and its dynamics was analyzed by time-lapse confocal microscopy for more than 100 min. Quantification of the relative fluorescence intensity in photoactivated canalicular areas (BC) and adjacent basolateral membrane regions after background subtraction (n = 14 cells) is shown.

(F) Reduced basolateral-to-apical transport of photoactivated ICAM-1-Δct-paGFP. Quantification of fluorescence in basolateral and canalicular (BC) regions adjacent to photoactivated areas after background subtraction (n = 15 cells) is shown.

(G) HepG2 cells expressing radixin (RDX)-YFP or ezrin-GFP were left untreated or depolarized by PMA treatment for 4 hr, fixed, and stained for ICAM-1.

(H) Endogenous ICAM-1 was engaged with specific mouse antibodies in the cold for 30 min and crosslinked with secondary antibodies for 30 min at 37°C (X-ICAM-1) in cells expressing the indicated fluorescent proteins. The graph shows the Manders coefficient, which measures the overlap between the distribution of X-ICAM-1 and the indicated fluorescent proteins. The ratio of YFP/GFP-positive pixels that are also positive for clustered ICAM-1 is shown. *p = 0.028; **p = 0.002; n = 3.

(I) HepG2 cells stably expressing ICAM-1-GFP or ICAM-1-Δct-GFP were knocked down for endogenous ICAM-1 for 72 hr and subjected to ICAM-1 crosslinking (X-ICAM-1), fixed, and stained for p-ERMs. The Manders coefficient shows the GFP staining that was positive for p-ERM staining. *p = 0.013; n = 3.

(J) Radixin and ezrin associate with the ICAM-1 cytoplasmic tail. Top, Coomassie blue staining of the indicated recombinant GST proteins. Bottom, pull-downs with recombinant GST alone and GST containing the ICAM-1 cytoplasmic segment were subjected to western blotting for the indicated ERM proteins.

(K) HepG2 cells stably expressing ICAM-1-K>L-GFP were knocked down for endogenous ICAM-1 and subjected to ICAM-1 crosslinking (X-ICAM-1), fixed, and stained for p-ERMs.

(L) Parallel quantification of the basolateral index for ICAM-1-GFP and ICAM-1-K>L-GFP. *p = 0.0083; n = 7. Bars show the mean + SEM. Scale bars represent 10 μm.

See also Figure S3 and Movies S5 and S6.

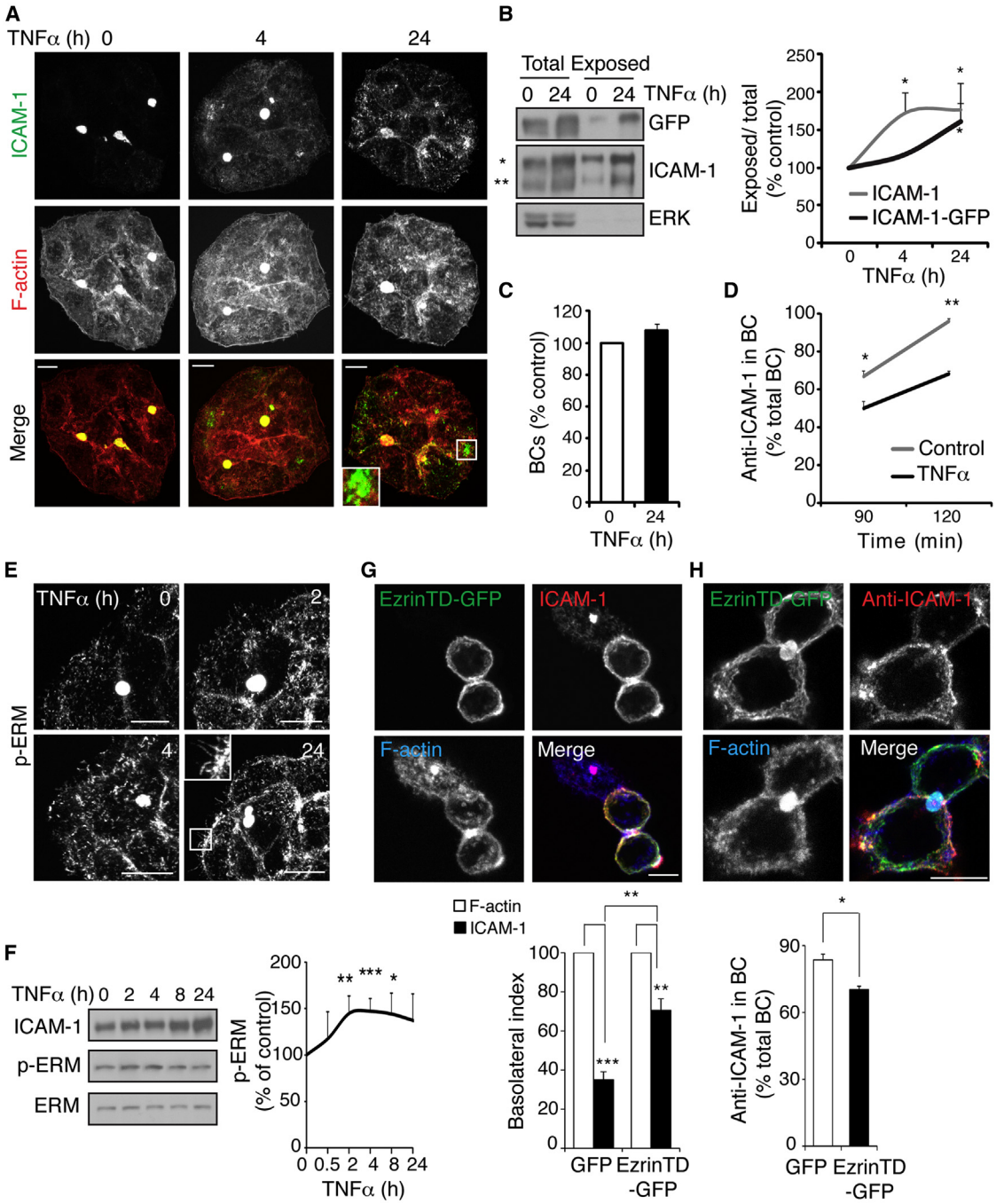

Figure 6. TNF-α Increases ICAM-1 Basolateral Localization through Basolateral Activation of ERM Proteins

(A–E) HepG2 cells or HepG2 stably expressing ICAM-1-GFP were grown for 72 hr and then stimulated with 50 ng/ml TNF-α for the indicated times.

(A) HepG2 cells were fixed and stained for endogenous ICAM-1 and F-actin. The enlarged area shows basolateral ICAM-1- and F-actin-rich clusters in TNF-α-stimulated cells.

(B) TNF-α-stimulated cells were labeled with sulfo-NHS-biotin, followed by neutravidin pull-down assays (Exposed), as in Figure 2. Left, western blot for the indicated proteins in HepG2 cells expressing ICAM-1-GFP. Asterisks indicate the bands corresponding to ICAM-1-GFP (*) and endogenous ICAM-1 (**). Right graph: exposed-to-total ratios were calculated for endogenous ICAM-1 in HepG2 cells and for ICAM-1-GFP in HepG2-ICAM-1-GFP cells, and expressed as the percentage relative to unstimulated cells. *p = 0.044, n = 3; **p = 0.036, n = 4; ***p = 0.028; n = 5.

(C) F-actin- and ICAM-1-rich canalicular structures were quantified in unstimulated cells and cells stimulated with TNF-α for 24 hr.

(D) HepG2-ICAM-1-GFP was left unstimulated or stimulated for 24 hr with TNF-α. Cells were basolaterally labeled with anti-ICAM-1 antibody and incubated at 37°C for the indicated times. The percentage of BCs that were positive for basolateral ICAM-1 was quantified. *p = 0.011; **p = 6.925×10^{-5}; n = 3.

(legend continued on next page)

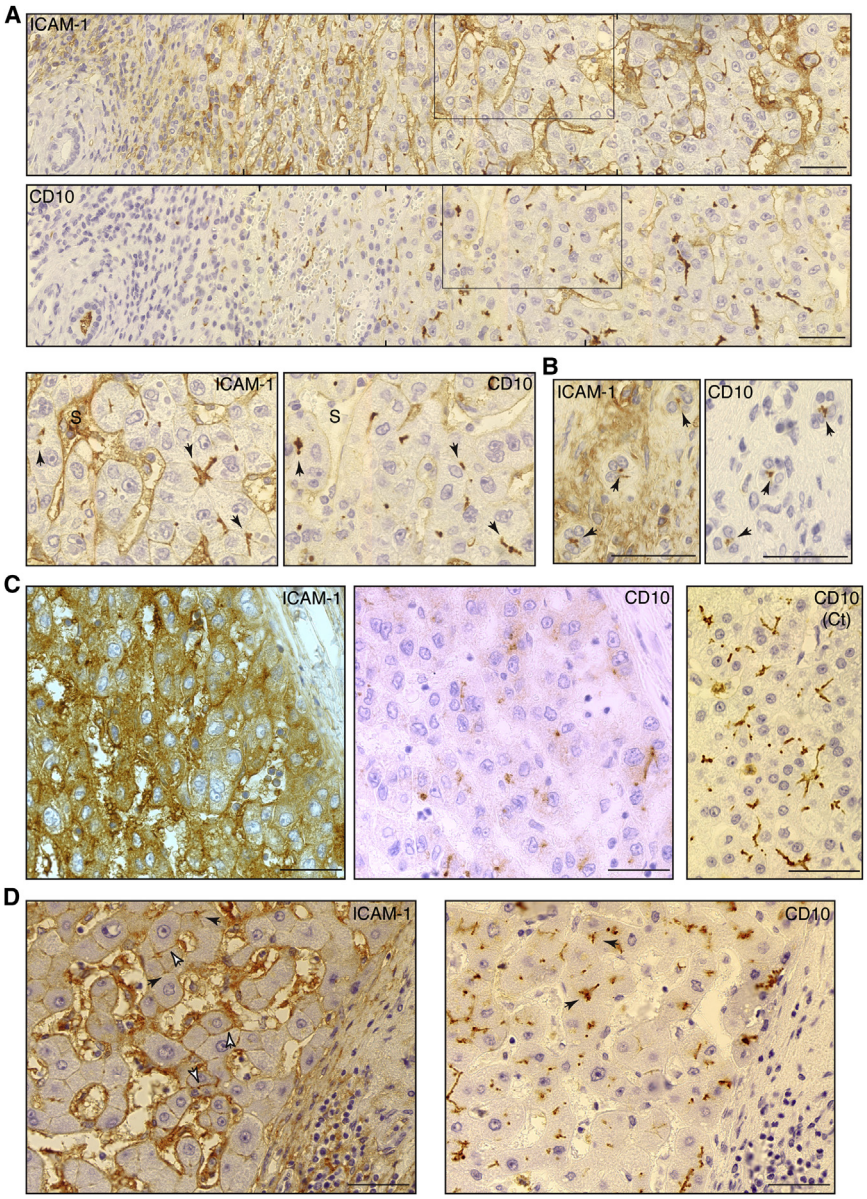

Figure 7. ICAM-1 Distribution in Human Livers with Chronic HCV and HBV Infection

(A–C) Immunohistochemical staining of consecutive paraffin sections shows the distribution of ICAM-1 in the liver parenchyma of a patient with chronic HCV infection.

(A and B) Four overlapping fields from two consecutive paraffin sections stained for ICAM-1 and CD10. The enlarged boxed areas show the canalicular distribution of ICAM-1 and CD10 (arrows, bottom). S, sinusoid.

(B) Apical distribution of ICAM-1 and CD10 in bile ducts (arrows).

(C) ICAM-1 distribution in another region of the same liver parenchyma, in which hepatic cells have lost their apicobasal architecture as revealed by weaker CD10 staining (left and center) compared with control samples (Ct) from healthy donors (right). Note the unpolarized distribution of ICAM-1. A similar heterogeneous distribution of hepatic ICAM-1 was observed in tissue sections from livers chronically infected with HBV.

(D) Immunohistochemical staining of consecutive liver sections stained for ICAM-1 and CD10, from a patient with chronic HBV infection. White arrows point to hepatocytes with unpolarized ICAM-1 and polarized CD10 distribution. Black arrows point to hepatocytes with canalicular ICAM-1 staining. Unpolarized distribution of ICAM-1 in areas in which polarized CD10 was also observed in HCV-infected liver parenchyma. Scale bars represent 10 μm.

See also Figure S5.

Adhesion Assays

HepG2 cells were plated onto 24-well plates (2.5×10^5/well) for 48 hr. T cells were labeled with 0.5 μM calcein for 30 min, blocked, and extensively rinsed with medium. HepG2 cells subjected to different treatments were thoroughly rinsed and then 3×10^5 T cells per well were added for 15 min. After washing, fluorescence from calcein-labeled, adhered T cells was detected with a fluorescent microplate reader (FLUOstar OPTIMA; BMG Labtech). Alternatively, adhesion experiments were also assayed using a confocal microscope to count calcein- or CMTMR-labeled T cells that adhered to HepG2 cell colonies. T cell adhesion was blocked by incubation of HepG2 cells with 10 μg/ml of mouse anti-ICAM-1 antibody or T cells with 15 μg/ml of mouse anti-CD11/CD18 (LFA-1) antibody 30 min before adhesion assays were conducted.

Labeling of Exposed Surface Receptors

HepG2 cells were subjected to various treatments to modulate polarity, rinsed with PBS Ca^{2+}/Mg^{++}, and incubated for 20 min with 250 μg/ml of sulfo-NHS-biotin. The cells were washed and traces of unbound biotin were blocked by incubation for 20 min with Dulbecco's modified Eagle's medium plus 10% fetal calf serum. Labeled HepG2 cells were then lysed with 1% TX-100 in TNE containing protease and phosphatase inhibitors, and neutravidin-agarose pull-down was performed. All of these procedures were performed at 4°C.

(E) p-ERM staining in HepG2 cells upon TNF-α stimulation. The enlarged area shows microvilli-like structures in basolateral membrane regions.

(F) Western blot of ICAM-1 and p-ERM (top) and quantification of the p-ERM increase with respect to unstimulated cells (bottom). *p = 0.042; **p = 0.019; ***p = 0.001; n = 7.

(G) Transfection of a constitutive active mutant form of ERMs (ezrin-TD-GFP) is sufficient to increase basolateral localization of ICAM-1 in polarized HepG2 cells. The graph shows the ICAM-1 basolateral index normalized with respect to the F-actin index. *p = 0.026; **p = 0.005; ***p = 0.001; n = 3. Bars show the mean + SEM.

(H) The percentage of BCs that were positive for basolateral ICAM-1 90 min after immunolabeling is reduced upon ezrin-TD-GFP expression. *p = 0.0003; n = 4. Scale bars represent 10 μm.

See also Figure S4 and Movie S7.

Photoactivation and Time-Lapse Confocal Microscopy

HepG2 cells stably expressing photoactivatable ICAM-1-paGFP or ICAM-1-Δct-paGFP were seeded on a 35-mm glass-bottom culture dish and cultured for 2 days. Imaging was performed with a 63× water immersion objective lens (Plan-Apochromat; NA 1.0) on an inverted microscope (AxioObserver) equipped with a confocal scanning system (LSM710; Zeiss). Cells were imaged in phenol-red-free HEPES 20 mM Hank's balanced salt solution medium in a heated chamber at 37°C. A 405 nm laser was used to photoconvert ICAM-1-paGFP within the defined area of interest. For short videos (up to 10 min total duration) photoactivation was performed using a single pulse at 40% laser power, followed by time series imaging at 3 s per frame. For videos up to 120 min, the basolateral or apical domain was photoactivated using several pulses at 40% laser power or one single-pulse at 20% laser power, respectively, followed by two to three frames at maximum scan speed, and then 1–2 hr at 10 min per frame. Two images were acquired before photoconversion and their average intensity was taken as background and subtracted from the fluorescence intensity obtained after photoactivation, and then normalized to the intensity obtained in the first image recorded after photoconversion. Images were analyzed using ZEN 2010 (Carl Zeiss) and ImageJ (NIH) software.

SUPPLEMENTAL INFORMATION

Supplemental Information includes Supplemental Experimental Procedures, five figures, two tables, and seven movies and can be found with this article online at http://dx.doi.org/10.1016/j.celrep.2014.08.007.

ACKNOWLEDGMENTS

We thank the staff of the Optical and Confocal Microscopy Facility of the CBMSO for technical advice and Prof. C. Gamallo (Hospital de la Princesa, Madrid) for technical advice and helpful discussion regarding the immunohistochemical analysis. This work was supported by grants SAF2011-22624 (to J.M.), BFU2012-32532 and CSD2009-00016 (to M.A.A.), and BFU2011-22859 (to I.C.) from the Ministerio de Ciencia e Innovación; grant S2010/BMD-2305 from Comunidad de Madrid; and grant FIS PI10/00101 from the Ministerio Sanidad and Fundación Mutua Madrileña (to P.L.). N.R. is a recipient of a JAE predoctoral fellowship from the CSIC. B.M. is a recipient of an FPI fellowship from the MINECO.

Received: September 3, 2013
Revised: June 25, 2014
Accepted: August 4, 2014
Published: September 18, 2014

REFERENCES

Akkari, L., Grégoire, D., Floc'h, N., Moreau, M., Hernandez, C., Simonin, Y., Rosenberg, A.R., Lassus, P., and Hibner, U. (2012). Hepatitis C viral protein NS5A induces EMT and participates in oncogenic transformation of primary hepatocyte precursors. J. Hepatol. *57*, 1021–1028.

Aranda, J.F., Reglero-Real, N., Marcos-Ramiro, B., Ruiz-Sáenz, A., Fernández-Martín, L., Bernabé-Rubio, M., Kremer, L., Ridley, A.J., Correas, I., Alonso, M.A., and Millán, J. (2013). MYADM controls endothelial barrier function through ERM-dependent regulation of ICAM-1 expression. Mol. Biol. Cell *24*, 483–494.

Barreiro, O., Yanez-Mo, M., Serrador, J.M., Montoya, M.C., Vicente-Manzanares, M., Tejedor, R., Furthmayr, H., and Sanchez-Madrid, F. (2002). Dynamic interaction of VCAM-1 and ICAM-1 with moesin and ezrin in a novel endothelial docking structure for adherent leukocytes. J. Cell Biol. *157*, 1233–1245.

Bastaki, M., Braiterman, L.T., Johns, D.C., Chen, Y.H., and Hubbard, A.L. (2002). Absence of direct delivery for single transmembrane apical proteins or their "Secretory" forms in polarized hepatic cells. Mol. Biol. Cell *13*, 225–237.

Benedicto, I., Molina-Jiménez, F., Moreno-Otero, R., López-Cabrera, M., and Majano, P.L. (2011). Interplay among cellular polarization, lipoprotein metabolism and hepatitis C virus entry. World J. Gastroenterol. *17*, 2683–2690.

Carpén, O., Pallai, P., Staunton, D.E., and Springer, T.A. (1992). Association of intercellular adhesion molecule-1 (ICAM-1) with actin-containing cytoskeleton and alpha-actinin. J. Cell Biol. *118*, 1223–1234.

Chin, A.C., and Parkos, C.A. (2007). Pathobiology of neutrophil transepithelial migration: implications in mediating epithelial injury. Annu. Rev. Pathol. *2*, 111–143.

Delpino, M.V., Barrionuevo, P., Scian, R., Fossati, C.A., and Baldi, P.C. (2010). Brucella-infected hepatocytes mediate potentially tissue-damaging immune responses. J. Hepatol. *53*, 145–154.

Doi, T., Yamada, G., Mizuno, M., and Tsuji, T. (1994). Immunohistochemical study of the distribution of intercellular adhesion molecule-1 and lymphocyte function-associated antigen-1 in chronic type B hepatitis. J. Gastroenterol. *29*, 164–171.

Edwards, S., Lalor, P.F., Nash, G.B., Rainger, G.E., and Adams, D.H. (2005). Lymphocyte traffic through sinusoidal endothelial cells is regulated by hepatocytes. Hepatology *41*, 451–459.

Fu, D., Wakabayashi, Y., Lippincott-Schwartz, J., and Arias, I.M. (2011). Bile acid stimulates hepatocyte polarization through a cAMP-Epac-MEK-LKB1-AMPK pathway. Proc. Natl. Acad. Sci. USA *108*, 1403–1408.

Gilbert, S., Loranger, A., Lavoie, J.N., and Marceau, N. (2012). Cytoskeleton keratin regulation of FasR signaling through modulation of actin/ezrin interplay at lipid rafts in hepatocytes. Apoptosis *17*, 880–894.

Hiraoka, N. (2010). Tumor-infiltrating lymphocytes and hepatocellular carcinoma: molecular biology. Int. J. Clin. Oncol. *15*, 544–551.

Holz, L.E., Warren, A., Le Couteur, D.G., Bowen, D.G., and Bertolino, P. (2010). CD8+ T cell tolerance following antigen recognition on hepatocytes. J. Autoimmun. *34*, 15–22.

Hubbard, A.K., and Rothlein, R. (2000). Intercellular adhesion molecule-1 (ICAM-1) expression and cell signaling cascades. Free Radic. Biol. Med. *28*, 1379–1386.

Ivetic, A., and Ridley, A.J. (2004). Ezrin/radixin/moesin proteins and Rho GTPase signalling in leucocytes. Immunology *112*, 165–176.

Kang, T.W., Yevsa, T., Woller, N., Hoenicke, L., Wuestefeld, T., Dauch, D., Hohmeyer, A., Gereke, M., Rudalska, R., Potapova, A., et al. (2011). Senescence surveillance of pre-malignant hepatocytes limits liver cancer development. Nature *479*, 547–551.

Kanters, E., van Rijssel, J., Hensbergen, P.J., Hondius, D., Mul, F.P., Deelder, A.M., Sonnenberg, A., van Buul, J.D., and Hordijk, P.L. (2008). Filamin B mediates ICAM-1-driven leukocyte transendothelial migration. J. Biol. Chem. *283*, 31830–31839.

Kew, M.C. (2011). Hepatitis B virus x protein in the pathogenesis of hepatitis B virus-induced hepatocellular carcinoma. J. Gastroenterol. Hepatol. *26* (*Suppl 1*), 144–152.

Kikuchi, S., Hata, M., Fukumoto, K., Yamane, Y., Matsui, T., Tamura, A., Yonemura, S., Yamagishi, H., Keppler, D., Tsukita, S., and Tsukita, S. (2002). Radixin deficiency causes conjugated hyperbilirubinemia with loss of Mrp2 from bile canalicular membranes. Nat. Genet. *31*, 320–325.

Koss, M., Pfeiffer, G.R., 2nd, Wang, Y., Thomas, S.T., Yerukhimovich, M., Gaarde, W.A., Doerschuk, C.M., and Wang, Q. (2006). Ezrin/radixin/moesin proteins are phosphorylated by TNF-alpha and modulate permeability increases in human pulmonary microvascular endothelial cells. J. Immunol. *176*, 1218–1227.

Lee, N.P. (2012). The blood-biliary barrier, tight junctions and human liver diseases. Adv. Exp. Med. Biol. *763*, 171–185.

Madrid, R., Aranda, J.F., Rodríguez-Fraticelli, A.E., Ventimiglia, L., Andrés-Delgado, L., Shehata, M., Fanayan, S., Shahheydari, H., Gómez, S., Jiménez, A., et al. (2010). The formin INF2 regulates basolateral-to-apical transcytosis and lumen formation in association with Cdc42 and MAL2. Dev. Cell *18*, 814–827.

Martin-Belmonte, F., and Mostov, K. (2008). Regulation of cell polarity during epithelial morphogenesis. Curr. Opin. Cell Biol. *20*, 227–234.

Martin-Belmonte, F., Gassama, A., Datta, A., Yu, W., Rescher, U., Gerke, V., and Mostov, K. (2007). PTEN-mediated apical segregation of phosphoinositides controls epithelial morphogenesis through Cdc42. Cell *128*, 383–397.

Mashukova, A., Wald, F.A., and Salas, P.J. (2011). Tumor necrosis factor alpha and inflammation disrupt the polarity complex in intestinal epithelial cells by a posttranslational mechanism. Mol. Cell. Biol. *31*, 756–765.

McGettrick, H.M., Butler, L.M., Buckley, C.D., Rainger, G.E., and Nash, G.B. (2012). Tissue stroma as a regulator of leukocyte recruitment in inflammation. J. Leukoc. Biol. *91*, 385–400.

Mee, C.J., Farquhar, M.J., Harris, H.J., Hu, K., Ramma, W., Ahmed, A., Maurel, P., Bicknell, R., Balfe, P., and McKeating, J.A. (2010). Hepatitis C virus infection reduces hepatocellular polarity in a vascular endothelial growth factor-dependent manner. Gastroenterology *138*, 1134–1142.

Meijne, A.M., Driessens, M.H., La Rivière, G., Casey, D., Feltkamp, C.A., and Roos, E. (1994). LFA-1 integrin redistribution during T-cell hybridoma invasion of hepatocyte cultures and manganese-induced adhesion to ICAM-1. J. Cell Sci. *107*, 2557–2566.

Millán, J., Hewlett, L., Glyn, M., Toomre, D., Clark, P., and Ridley, A.J. (2006). Lymphocyte transcellular migration occurs through recruitment of endothelial ICAM-1 to caveola- and F-actin-rich domains. Nat. Cell Biol. *8*, 113–123.

Morita, M., Watanabe, Y., and Akaike, T. (1994). Inflammatory cytokines up-regulate intercellular adhesion molecule-1 expression on primary cultured mouse hepatocytes and T-lymphocyte adhesion. Hepatology *19*, 426–431.

Nagendra, A.R., Mickelson, J.K., and Smith, C.W. (1997). CD18 integrin and CD54-dependent neutrophil adhesion to cytokine-stimulated human hepatocytes. Am. J. Physiol. *272*, G408–G416.

Oh, H.M., Lee, S., Na, B.R., Wee, H., Kim, S.H., Choi, S.C., Lee, K.M., and Jun, C.D. (2007). RKIKK motif in the intracellular domain is critical for spatial and dynamic organization of ICAM-1: functional implication for the leukocyte adhesion and transmigration. Mol. Biol. Cell *18*, 2322–2335.

Parkos, C.A., Colgan, S.P., Diamond, M.S., Nusrat, A., Liang, T.W., Springer, T.A., and Madara, J.L. (1996). Expression and polarization of intercellular adhesion molecule-1 on human intestinal epithelia: consequences for CD11b/CD18-mediated interactions with neutrophils. Mol. Med. *2*, 489–505.

Patterson, G.H., and Lippincott-Schwartz, J. (2002). A photoactivatable GFP for selective photolabeling of proteins and cells. Science *297*, 1873–1877.

Reglero-Real, N., Marcos-Ramiro, B., and Millán, J. (2012). Endothelial membrane reorganization during leukocyte extravasation. Cell. Mol. Life Sci. *69*, 3079–3099.

Shousha, S., Gadir, F., Peston, D., Bansi, D., Thillainaygam, A.V., and Murray-Lyon, I.M. (2004). CD10 immunostaining of bile canaliculi in liver biopsies: change of staining pattern with the development of cirrhosis. Histopathology *45*, 335–342.

Suda, J., Zhu, L., and Karvar, S. (2011). Phosphorylation of radixin regulates cell polarity and Mrp-2 distribution in hepatocytes. Am. J. Physiol. Cell Physiol. *300*, C416–C424.

Tolosa, L., Bonora-Centelles, A., Donato, M.T., Mirabet, V., Pareja, E., Negro, A., López, S., Castell, J.V., and Gómez-Lechón, M.J. (2011). Influence of platelet lysate on the recovery and metabolic performance of cryopreserved human hepatocytes upon thawing. Transplantation *91*, 1340–1346.

van Buul, J.D., Allingham, M.J., Samson, T., Meller, J., Boulter, E., García-Mata, R., and Burridge, K. (2007). RhoG regulates endothelial apical cup assembly downstream from ICAM1 engagement and is involved in leukocyte trans-endothelial migration. J. Cell Biol. *178*, 1279–1293.

van IJzendoorn, S.C., Zegers, M.M., Kok, J.W., and Hoekstra, D. (1997). Segregation of glucosylceramide and sphingomyelin occurs in the apical to basolateral transcytotic route in HepG2 cells. J. Cell Biol. *137*, 347–357.

Viswanatha, R., Ohouo, P.Y., Smolka, M.B., and Bretscher, A. (2012). Local phosphocycling mediated by LOK/SLK restricts ezrin function to the apical aspect of epithelial cells. J. Cell Biol. *199*, 969–984.

Wang, L., and Boyer, J.L. (2004). The maintenance and generation of membrane polarity in hepatocytes. Hepatology *39*, 892–899.

Wang, W., Soroka, C.J., Mennone, A., Rahner, C., Harry, K., Pypaert, M., and Boyer, J.L. (2006). Radixin is required to maintain apical canalicular membrane structure and function in rat hepatocytes. Gastroenterology *131*, 878–884.

Warren, A., Le Couteur, D.G., Fraser, R., Bowen, D.G., McCaughan, G.W., and Bertolino, P. (2006). T lymphocytes interact with hepatocytes through fenestrations in murine liver sinusoidal endothelial cells. Hepatology *44*, 1182–1190.

Weisz, O.A., and Rodriguez-Boulan, E. (2009). Apical trafficking in epithelial cells: signals, clusters and motors. J. Cell Sci. *122*, 4253–4266.

Wilson, G.K., Brimacombe, C.L., Rowe, I.A., Reynolds, G.M., Fletcher, N.F., Stamataki, Z., Bhogal, R.H., Simões, M.L., Ashcroft, M., Afford, S.C., et al. (2012). A dual role for hypoxia inducible factor-1α in the hepatitis C virus lifecycle and hepatoma migration. J. Hepatol. *56*, 803–809.

Zegers, M.M., and Hoekstra, D. (1997). Sphingolipid transport to the apical plasma membrane domain in human hepatoma cells is controlled by PKC and PKA activity: a correlation with cell polarity in HepG2 cells. J. Cell Biol. *138*, 307–321.

Zhu, H., Xia, M., Hou, M., Tang, Z., Li, Y., Ma, J., and Ling, W. (2005). Ox-LDL plays dual effect in modulating expression of inflammatory molecules through LOX-1 pathway in human umbilical vein endothelial cells. Front. Biosci. *10*, 2585–2594.